A petal-cylindrical seismic metamaterial occupying lowfrequency wide bandgaps in horizontally stratified soils

Muhammad Muzamil, Hongwu Yang, Rui Xu, Yi Zeng, Pai Peng, Qiujiao Du

A petal-cylindrical seismic metamaterial occupying low-frequency wide bandgaps in horizontally stratified soils

Muhammad Muzamil[a], Hongwu Yang[b], Rui Xu[a], Yi Zeng[c,] Pai Peng[a] and Qiujiao Du[a*]
[a] *School of Mathematics and Physics, China University of Geosciences, Wuhan 430074, China*
[b]*School of Civil Engineering and Mechanics, Huazhong University of Science and Technology- Wuhan 430074, China*
[c]*Université de Lorraine, CNRS, Institute Jean Lamour, Nancy 54500, France*

Abstract:

Earthquake prevention is of fundamental interest in seismic research area. Seismic metamaterials proved very useful for this purpose, but because they are mainly based on resonant structures, the working frequency bandwidth of these metamaterials is narrow. This work aims to increase the bandwidth by improving cylindrical resonant structure. Two types of cylindrical structures with four petals attached to the four sides of hollow and solid cylinders are proposed. Their bandgap properties have been investigated by using the finite element method. Particularly, considering more realistic site conditions for seismic surface wave propagation, we explored the properties of the proposed structures for horizontally stratified soils, besides homogenous soil. The results show that a low-frequency wide bandgap is provided in case of homogenous soil. Excitedly, in case of a stratified substrate, an additional bandgap is obtained in lower frequency region. Moreover, to confirm the feasibility of the proposed structures, the transmission coefficients for the finite unit cells are calculated for both homogenous and horizontally stratified soils along with the different directions. The finding substantiates that the finite system for stratified soils can effectively attenuate seismic surface waves within the two low-frequency bandgaps occupying the relative bandwidths of 154% and 81%.

Keywords: Seismic metamaterial, Earthquake prevention, Surface waves, Petal-cylindrical, Low frequency wide bandgap, Relative bandwidth

I. Introduction:

Preventive studies of earthquake engineering and Rayleigh surface waves have demonstrated that the two seismic practices are very significant for civil infrastructures. When earthquake waves come to the surface of the planet, energy spreads across the surface of the earth. The Rayleigh wave, one of the surface waves, is particularly dangerous to civil structures, with frequencies of 0.1 to 20 Hz, since the building or civil structure's resonance frequency lies precisely in this particular frequency range. Furthermore, it is difficult to monitor or separate these low-frequency surface waves using traditional techniques. The recently developed metamaterials are now opening up a new method for monitoring seismic waves in this century, followed by the presentation of metamaterials for extinction of seismic waves for the fortification of civil infrastructures [1].

Metamaterials, periodic or aperiodic composite structures, are manually developed or engineered structures with some unique properties which are not occurring in natural materials. With the proficiencies to deploy the waves propagation by their astonishing properties, i.e. negative refraction [2], self-collimation [3], and bandgaps [4], metamaterials have developed massive practical applications in optics, elastic mechanics and acoustic [5,6].

In previous studies, multiple types of waves have been under exploration like ultrasonic [7], acoustic [8], elastic [9], thermal [10] and electromagnetic waves [11]. Elastic metamaterials, particularly diminish and reflect elastic waves with distinctive bandgap property, and then bid a fresh way for earthquake deterrence. Exploring seismic wave mitigation, metamaterials is a successful technique owing to a fruitful tactic of wave manipulation at low frequencies. Seismic metamaterials (SMs) are defined as the elastic metamaterial application of diminishing of seismic waves. The seismic waves are attenuated as they pass to the SMs with bandgap properties. The resultant bandgaps from developing SMs, should mask the seismic waves' vital frequencies or even the resonant frequencies of the large-scal structures to ensure effective protection of buildings or other civil infrastructure.

In the earlier study, some researchers have confirmed that a periodic series of resonators/barriers mitigates field vibration. R.D. Woods et al. [12] presented the primary concept of periodically arranging the vertical holes for Rayleigh wave attenuation. F. Meseguer et al. [13] suggested theoretically to attenuate seismic surface acoustic waves by band gaps (BGs) created by

drilling enormous periodic holes in the ground. The projected holes had dimensions of the order of hundreds of meters in diameter and thousands of meters in depth. A scaled-down experiment of a marble quarry that was conducted in the kHz frequency range yielded the measurement of surface acoustic wave attenuation, which led to the development of such a radical recommended solution. A tentative progress of the seismic field test drives the excitement of research, which shows that cylindrical holes can reflect and absorb the incident seismic waves, evidencing the practicability of SMs as seismic shield. However, attenuation behavior of periodic arrangement of boreholes or pillars is originated from Bragg scattering, so the large-scale structures are unfavorable for anti-earthquake application in a low frequency range.

Currently, SMs can overcome this delinquent, based on the local resonance phenomenon, which can attenuate long-wavelength waves using small structures [14]. The mainstream of these SMs is often called the SMs of the subwavelength [15]. The first type of sub-wavelength SM can be referred to as the underground barrier of locally resonant metamaterials [16]. This type of small-scale underground SM is based on the resonance properties for long-wavelength seismic bulk wave attenuation. The second type of SMs consists typically of a periodic pillar-like structure on substratum, which primarily attenuate seismic surface waves in particular within the low-frequency spectrum. In the geophysical sense, the resonances in trees have been examined by Colombi et al. [17], which acts as locally resonant metamaterials for Rayleigh surface waves, and it indicates that the Rayleigh waves are attenuated strongly around 40 Hz and 110 Hz. The major seismic frequency spectrum are outside the bandgaps, but the observed results are still fascinating. The bulk waves transformed from Rayleigh surface waves due to the existence of local resonance phenomenon in an established meta-barriers, infiltrate the ground deeply [18]. Pu and Shi [19] have recently investigated many forms of periodic barriers to alleviate train-induced surface waves. The practicability of the H-fractal resonance for seismic wave attenuation was explored by [20]. Du et al. [20] and Miniaci et al.[21] examined the viability of a novel structure with a self-similar geometry repeated at various scales based on hierarchical design of the unit cell. The findings demonstrated how the addition of hierarchy enables the conception of unit cells with reduced size relative to wavelength while keeping the same or better isolation effectiveness at frequencies of importance for earthquake engineering. The SMs in these studies have achieved influential protection of buildings for attenuating the low-frequency seismic waves. However, the seismic wave attenuation region is comparatively small, and our research aims to increase the bandwidth

by optimizing the section shape of the resonators. Inspired by previous work [22, 23] we for the first time make attempt to introduce petal-like section into SM instead of ordinary cylinder, and investigate the bandgap characteristics of petal-like SM adopting three-dimensional (3D) modeling. Meanwhile, we consider the conditions of the site to be more practical because the soil is critical in the propagation and coupling of surface waves with resonators. In this paper, we propose two different types of cylindrical resonators on both homogenous [20] and six-layered soil [24] substrates, respectively. Geometrically, the two resonant unit cells are hollow and solid cylinders with four petals attached to their four sides.

Numerical simulation is used for the proposed model to study the bandgap properties and generation mechanism. In particular, the bandgap structures of both proposed samples for homogenous and stratified soils are discussed and their comparison is explained. A larger impedance mismatch for stratified soils between the resonators and substrate results in a wider bandgap, and the values imply the low-frequency regime. Furthermore, through a frequency domain analysis, the transmission of finite SMs is calculated, and verify the feasibility of the proposed model's effective attenuation of surface waves. A detailed analysis of geometrical and material parameters is explained in the last section.

II. Models and method

An improved hollow cylindrical unit cell by uniformly adding four petals to its four sides, termed petal-cylindrical unit here, is proposed as an SM unit, shown in Figs. 1(a-d). The unit cells (homogenous and layered substrate) in Figs. 1(c) and 1(d) are placed in a square lattice on the surface of a semi-infinite substrate. We chose a lattice constant of a = 2.5m and a height of the unit h= 5a corresponding to the seismic surface waves of 0.1–20 Hz that destruct structures, leading to a wavelength range of several hundred meters. Figures 1(a) and (b) show a three-dimensional (3D) illustration as well as a y-z cross-section diagram of the hollow petal-cylindrical unit cell. For the inner hollow cylindrical part, r_1 and r_2 are the inner and outer radii, respectively, and its thickness is $w = r_2$-r_1. The outer radius and thickness of the petals are R and d, respectively. The geometric parameters of the hollow petal-cylindrical structure are enlisted in Table 1. In the simulation, a plate under the petal-cylindrical structure is installed as a substrate for a half-space setting. The depth of substrate is sufficient enough for the surface wave to be separated from the Lamb waves,

while the waves are diminished exponentially alongside the depth. In view of the practical application, steel is considered to be the structure, and soil is considered to be the substrate, shown in Table 2 and Table 3.

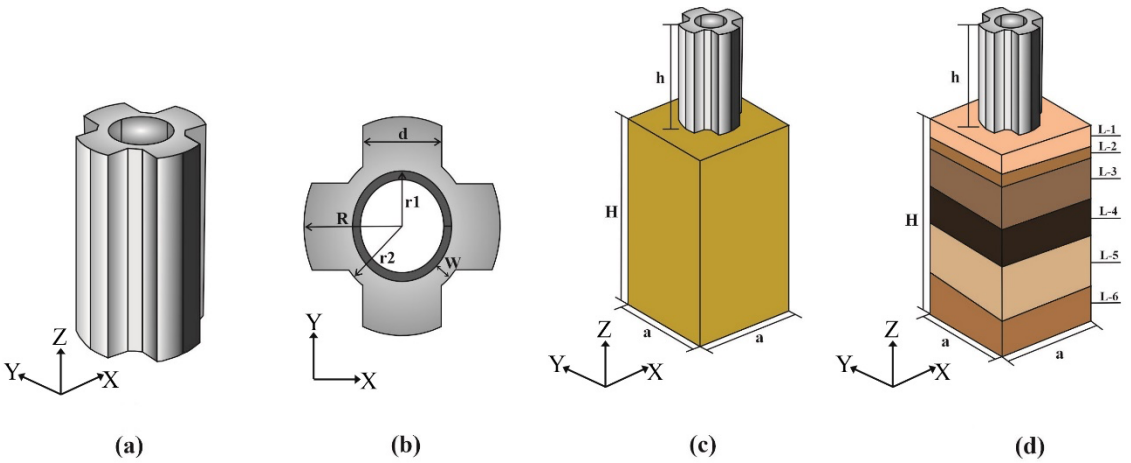

Fig. 1: Schematic illustration of the hollow petal-cylindrical unit cell (a) 3D view, (b) y-z or 2D view, (c) and (d) on the substrate for dispersion curve calculation. Note the yellow and multi-colored areas represent the homogenous and stratified substrates, and the grey color represents steel.

In Figs. 2(a-d), the second proposed sample called as solid petal-cylindrical structure is shown. The structure units are arranged in a square lattice on semi-infinite homogenous and layered substrates as shown in Figs. 2(c) and (d), having the same geometrical and material parameters as the hollow petal-cylindrical structure. We continue to use the structure's lattice constant $a = 2.5$m and height $h = 5a$. The 3D and y-z cross-section views of the solid petal-cylindrical unit cell are seen in Figs. 2(a) and (b), respectively. The second sample is a steel-filled petal-cylindrical structure. Of course, the filling material can also be other common materials, such as concrete.

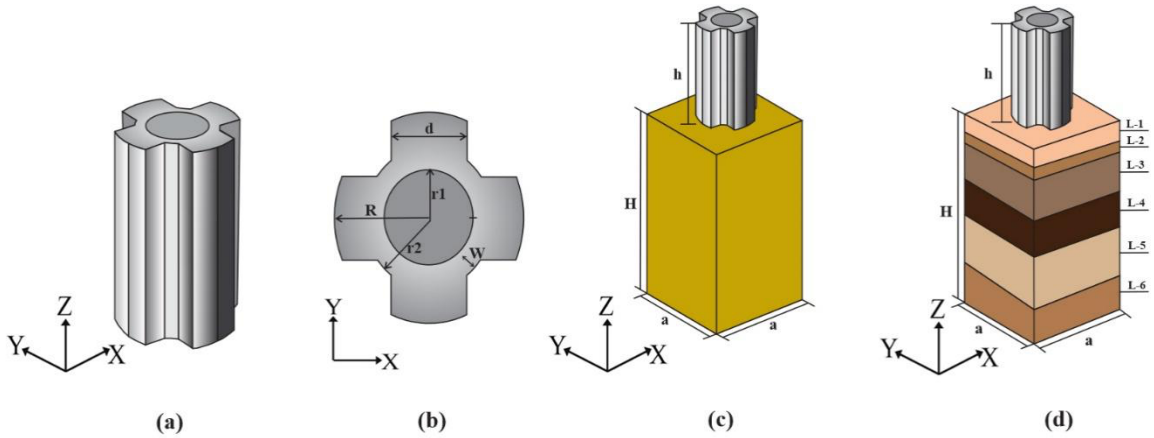

Fig. 2: Schematic illustration of the solid cylindrical unit cell (a) 3D view (b) y-z or 2D view, (c) and (d) on the substrate for dispersion curve calculation. Note the yellow and multi-colored areas represent the homogenous and stratified substrates, respectively, and the grey color represents steel.

Table 1: Geometrical parameters of the proposed unit cells

a	h	H	r_1	R	r_2	d	w
2.5 m	5a	20a	$a/8$	a/4	a/6	a/5	r_2-r_1

Table 2:Material parameters of the hollow and solid cylindrical unit cells

Material type	Density ρ (kg/m^3)	Young's modulus (Pa)	Poisson's ratio
Steel	7784	2.07×10^{11}	0.3

To check the feasibility of the proposed unit models on two different substrates, the homogenous and multiple-layered soil substrates are used for the propagation of surface waves. The properties of both selected substrates are shown in table 3. All components, including soils and steel, are considered linear elastic, iaotropic and homogeneous.

Table 3:homogenous and stratified soil properties

Properties of multiple layered soils [24]					
No.	Soil type	Thickness(m)	Density(kg/m^3)	Young's modulus E (Pa)	Poisson's ratio
1	Fill	3	1840	3.7×10^7	0.4
2	Clay Silt	2	1849	4.4×10^7	0.4
3	Sandy Silt	10	1898	5.3×10^7	0.4
4	Silt	10	1908	1.41×10^8	0.45
5	Sandy Silt	15	1847	9.0×10^7	0.45
6	Silty Clay	10	1857	1.55×10^8	0.45
Properties of homogenous soil [20]					
1	Homogenous soil layer	30	1800	3.0×10^{11}	0.3

III. Method:

We suppose the surface waves propagation along the *x*-*y* plane, while the *z*-axis is taken along height direction, so the governing equation can be written as follows

$$\rho\ddot{u} - \nabla \cdot (C : \nabla u) = 0 \qquad (1)$$

Where ρ is the density of constituent material, the displacement vector $u = [u_x, u_y, u_z]^T$, where u_x, u_y and u_z are the displacement components in three directions of the Cartesian coordinate system, and the superimposed point above the vector u is the time derivative. ∇ is the inverted trigonometric operator and C represents the elastic tensor.

To determine the band structure diagram of the metamaterial with infinite period structure, we set Bloch periodic boundary conditions on the four lateral sides of the unit cell along the *x*- and *y*- axis directions to solve the equation (1), namely the displacement amplitude condition[20].

$$u(r + a) = e^{ik\cdot a}u(r) \qquad (2)$$

Where r denotes the position vector, $i = \sqrt{-1}$, k is the Bloch wave vector specified in the first irreducible Brillouin zone (FIBZ), and a represents the lattice constant. The standard eigenvalue problem is obtained by removing the displacement amplitude condition from the governing equation.

$$(K - \omega^2 M)u = 0 \qquad (3)$$

where K and M are the global stiffness and mass operators related to the wave vector k, and ω is the angular frequency. For this investigation, we use the finite element method to scan the wave vector k along with Γ-X-M-Γ directions in the FIBZ, and then we solve the unknowns ω and u. The solution of eigenvalue problems results in the eigenvectors for the displacement field modes. The FIBZ for periodic composition with square lattice is shown in Fig. 3. The Brillouin zones are primitive Wigner-Seitz cells in the reciprocal lattice. The first Brillouin zone is the smallest volume completely encompassed by planes that are the perpendicular bisectors of the sketched reciprocal lattice vectors [25].

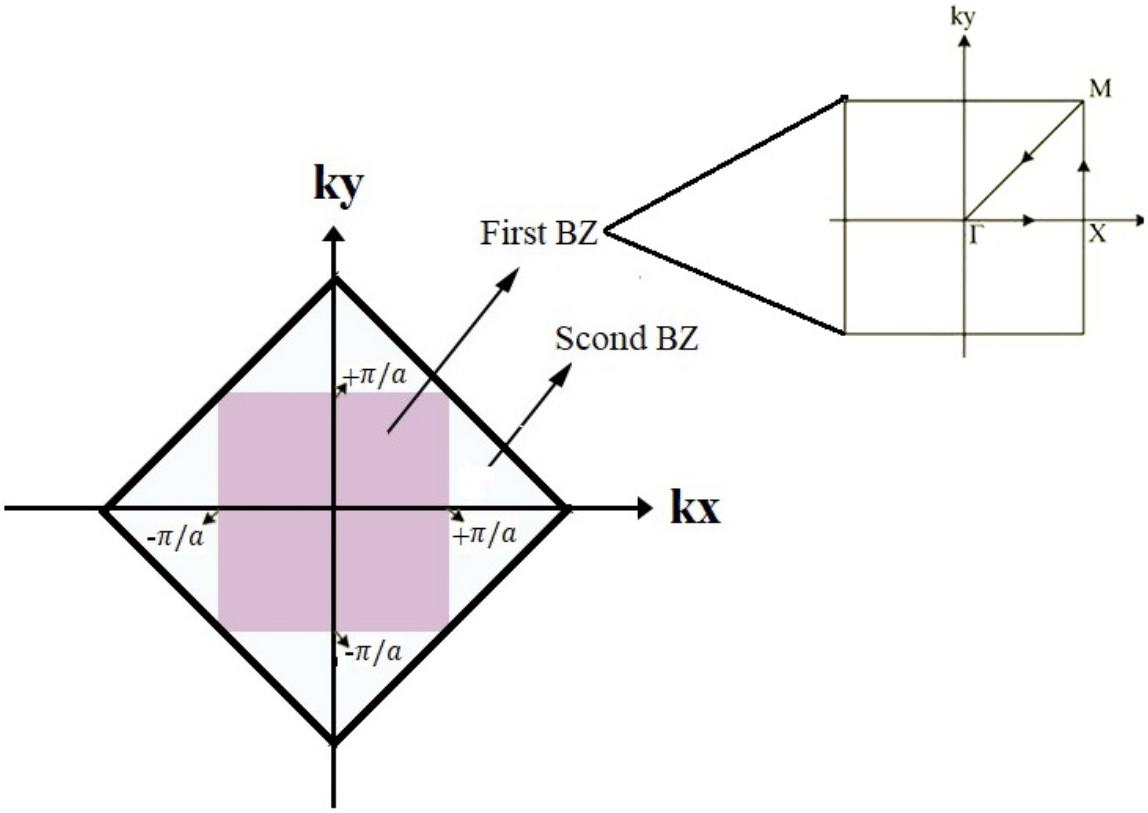

Fig. 3: Brillouin Zones and the first IBZ for the periodic components of a square lattice.

IV. Results and discussion

We compute the band structures of the considered SMs using the Floquet-Bloch theory and the finite element method. The band structures and eigenmodes for the models presented in Figs. 1(c) and (d) and Figs. 2 (c) and (d) are discussed below. The periodic conditions are applied at four

lateral boundaries, the cell's top contains a free boundary condition and the base is with a fixed boundary condition. The individual eigenfrequencies and eigenmodes as described in Figs. 4(a) and (b), are obtained by sweeping the wave vectors along the Γ-X-M-Γ path in the FIBZ. The surface wave modes can be sorted using the sound cone, while the green area represents the radiated field beyond the sound cone, which includes the bulk and high-frequency pseudo surface wave modes [26].

From the band structure of the hollow petal-cylindrical SM on a homogenous soil substrate, we find a wide bandgap with a width of 6.38Hz appearing from 6.62 Hz to 13.0 Hz, as shown in Fig. 4(a). The relative bandwidth is a significant parameter to estimating the property of the bandgap, which is well defined as $2(f_2-f_1)/(f_1+f_2)$, where f_2 and f_1 are the upper and lower edge frequencies of the bandgap. This proposed SM has a relative bandwidth of up to 64.6%.

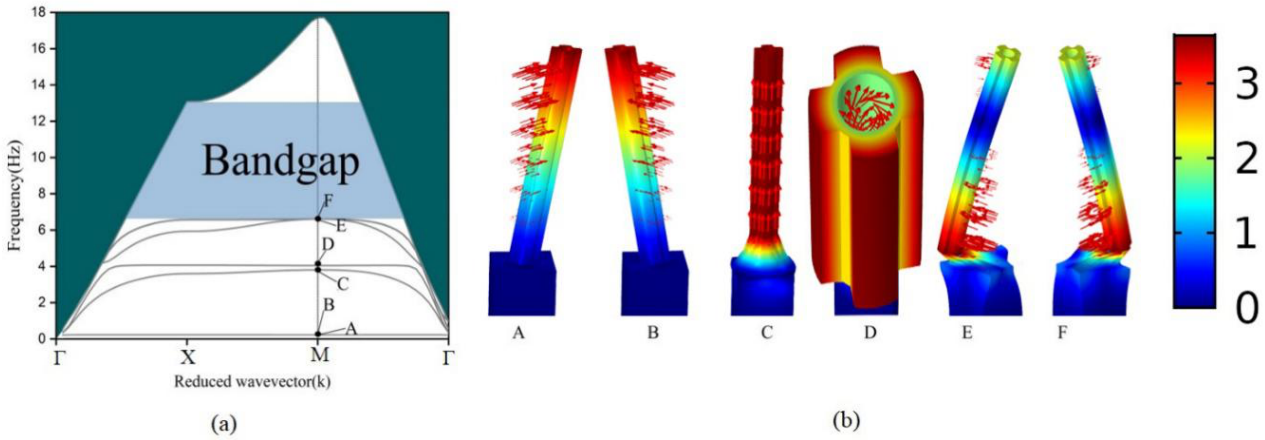

Fig. 4: (a) The band structure of hollow petal-cylindrical SM on a homogenous soil substrate and (b) A-F are the corresponding vibrational modes.

From the band structure of the solid petal-cylindrical SM on a homogenous soil layer, we also find a wide bandgap as shown in Fig. 5(a). The bandgap with a width of 7.41 Hz appears from 5.59 Hz to 13.0 Hz corresponding to a relative bandwidth of up to 80%, which is relatively larger as compared to the hollow petal-cylindrical structure as shown in Fig. 4.

The vibrational modes of the lower and upper edges, highlighted by the black points in Figs. 4(a) and 5(a) demonstrate the generation mechanism of the above bandgaps. The displacement fields of the eigenmodes (A–F) for both hollow and solid petal-cylindrical SMs are shown in Figs. 4(b) and 5(b). The color and arrow schemes show the magnitude and direction of the displacement vectors of the eigenmodes. The resonant modes are observed to be the same for

both types of SMs. A larger impedance malfunction between soil media and unit cells for the solid cylindrical case leads to a stronger local resonance which yielded a broader low-frequency bandgap.

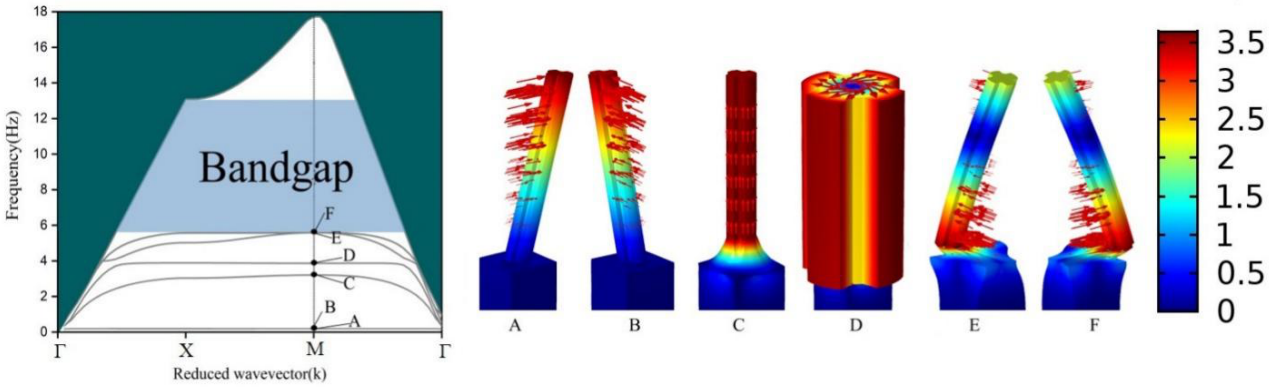

Fig. 5: (a) The band structure of a solid petal-cylindrical SM on a homogenous soil substrate (b) A-F are the corresponding vibrational modes.

After the band structures are discussed on the homogenous soil substrate, we replace the soil medium with six-layered soils, while the geometric parameters are kept the same as reported in Table 1. And we calculate the band structures for hollow and solid petal-cylindrical SMs on the stratified soils. For the hollow petal-cylindrical SM on the six-layered soils, we obtain one small bandgap in a lower frequency range from 0.33 Hz to 2.28 Hz, and a wider bandgap from 8.85 Hz to 17.8 Hz, as shown in Fig. 6(a). Its relative bandwidths at the two central frequencies of 1.3 Hz and 13.3 Hz are about 149% and 67%, respectively.

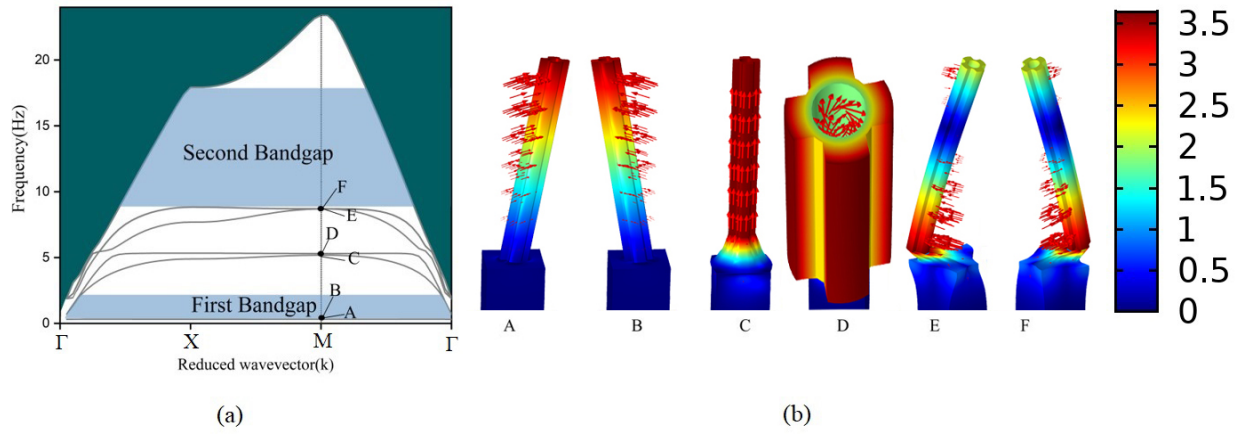

Fig. 6: (a) The band structure of hollow petal-cylindrical SM on a stratified substrate (b) A-F are the corresponding vibrational modes.

The band structure for solid petal-cylindrical SM on a stratified substrate is shown in Fig.

7(a) and the marked eigenmodes from A-F are given in Fig. 7(b). Moreover, two local resonance bandgaps in the frequency spectrum ranging from 0.25-1.93 Hz and 7.49-17.8 Hz are achieved. The relative bandwidths are 154% and 81% and they are larger than that for hollow petal-cylindrical SM. More importantly, they are relatively greater as compared to the previous studies (bandwidths of less than 45%) [18,27,28].

Next, to further investigate how to achieve larger bandgaps for the petal-cylindrical SMs, the vibrational eigenmodes (A-F) highlighted by the black dots in Figs. 6(a) and 7(a) are explored, namely the displacement fields of the eigenmodes, as shown in Fig. 6(b) and in Fig. 7(b). The color and arrow schematics specify the magnitude and direction of the displacement vectors of the eigenmodes. Interestingly, a larger relative bandwidth on the stratified substrate than on the homogeneous substrate is obtained because of a coupling of wave modes between surface wave and longitudinal wave that is regulated by a greater impedance misalignment between the resonator and substratum. It shows that the variation in the substrate's material properties influences the eigenfrequency of the resonant structure. Thus, we can deduce that the bandwidth can vary depending on the form and properties of the cohesive soils for a same resonator.

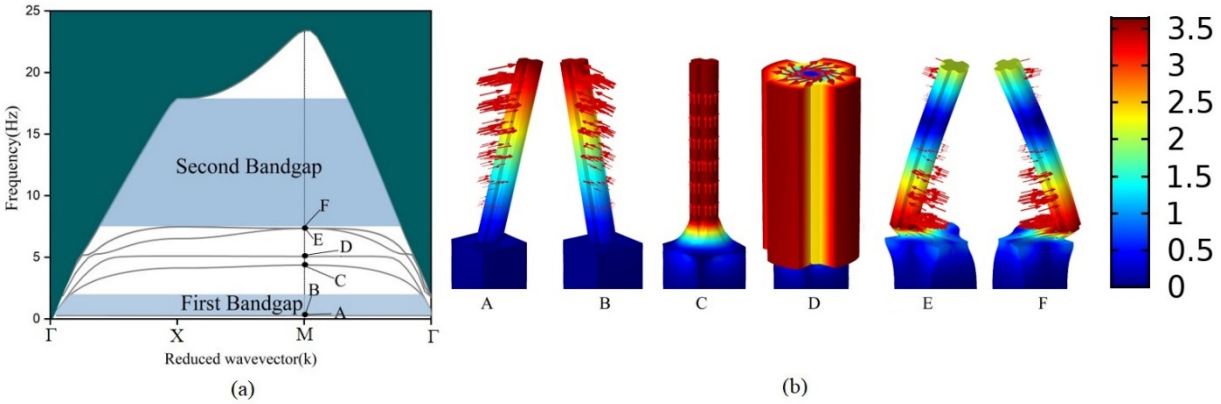

Fig. 7: (a) The band structure of solid cylindrical SM on a stratified substrate (b) A-F are the corresponding vibrational modes.

From the mode shapes shown in Figs. 4(b), 5(b), 6(b), and 7(b), which are highlighted in four band structure diagrams in Figs. 4(a), 5(a), 6(a) and 7(a), we observe that the SMs develop resonance modes, which confine the energy inside the system and the substrate. Commensurately, modes A and B are bending vibrational modes in the *x* and *y* directions, respectively, and the first and second dispersion curves are at around the same frequency, while another mode C is primarily longitudinal vibration along the *z*-axis. In contrast, mode D referring to the fourth curve of the band configuration manifests as rotation vibration, meanwhile, the cylinder is amplified in the *x*-

254 *y* cross-section. Eventually, complex rotation modes at E and F points are released, which are
255 regarded as string vibrations. We can surmise from the above analysis that a framework for the
256 formation of the bandgap of the proposed metamaterial is primarily due to the local resonance of
257 the structure.

258 **V. Transmission characteristics of finite systems**

259 We are using the finite arrangement of unit cells to measure the transmission coefficient of
260 the surface waves to further validate the shielding of the predicted SMs. The model consists of
261 units of SMs, substrates and perfectly matched layers (PML) [29] can be seen in Fig. 8. Five SM
262 units are placed periodically along the *x*-direction, adopting the lattice constant as a unit of length
263 and conforming to the SM unit geometrical and material parameters mentioned above in Tables 1-
264 3. The substrate thickness $H = 20a$, is retained to estimate a half-space computing field. Periodic
265 boundary conditions in the *y*-direction are applied to enforce periodic structures, and a source of a
266 line that excites the Rayleigh waves is represented shown in Figs. 8 (a) and (b). PMLs are applied
267 to all boundaries of substrates except the upper boundary where free boundary condition is applied.
268 Inherent yet unreasonable reflections generated by the scattering of waves are eliminated by PMLs
269 with a thickness of *3a*. The distance from the line source to the first SM unit is *20a*, which is
270 sufficiently long to separate the bulk waves from the desired surface waves in the *x*-direction. The
271 PML consists of a nonphysical substance that offers "active" absorption of fields and contains both
272 passive loss and dependent sources. It has been used in electromagnetic applications where it has
273 yielded good results over a broad spectrum of angles and frequencies.

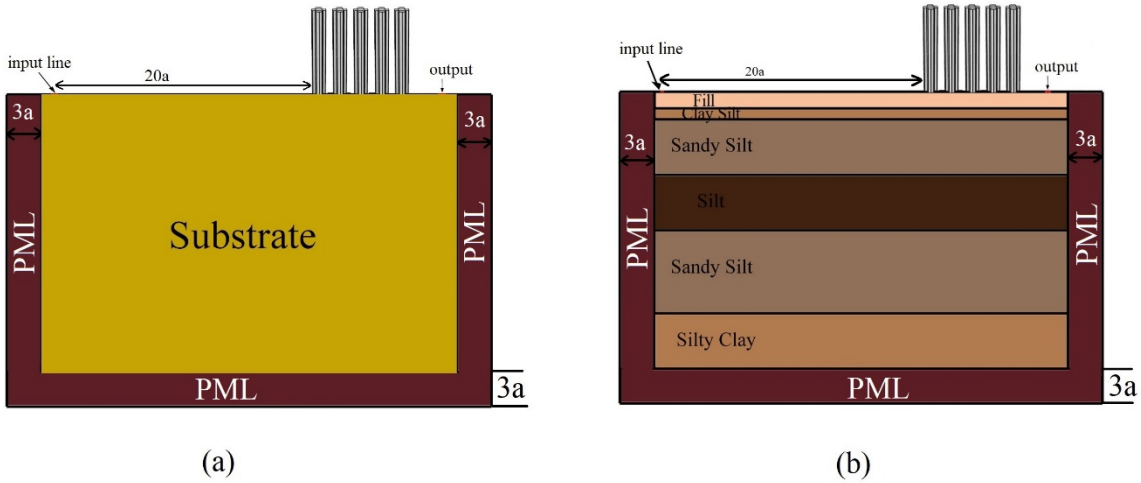

274

275 *Fig. 8: Schematic of the finite structures on homogenous and stratified soils with periodic boundary conditions in the y-direction*

for the transmission spectrum coefficients. The yellow (a) and multi-colored areas (b) represent the soils and the dark brown area is to represent PML. The silver cylinders on the substrates are the SMs units.

Hither, we make transmission calculations in the first Brillouin zone from the three symmetrical directions that resemble ΓX, XM, and MΓ directions and obtain the frequency response functions (FRFs), which are calculated as $20log(u_1/u_0)$, as shown in Figs. 9(a-d). u_1 is well defined as the displacement at the point next to the SMs, and u_0 is defined as the displacement at the same point without the SMs. Both the points are indicated in Figs. 8(a) and (b) as outputs. From the FRFs in Figs. 9(a) and (b), we can observe one complete attenuation zone from 6.62 Hz to 13 Hz and 5.59 Hz to 13.0 Hz, respectively, which are consistent with the band structure results shown in Figs. 3(a) and 4(a). It is worth noting that we can achieve two complete attenuation zones (CAZs) from 0.33 Hz to 2.28 Hz and from 8.85 Hz to 17.8 Hz in the Fig. 9(c), two CAZs from 0.25 Hz to 1.93 Hz and from 7.49 Hz to 17.8 Hz in the Fig. 9(d), respectively, which are consistent with the results expressed in Figs. 6(a) and 7(a).

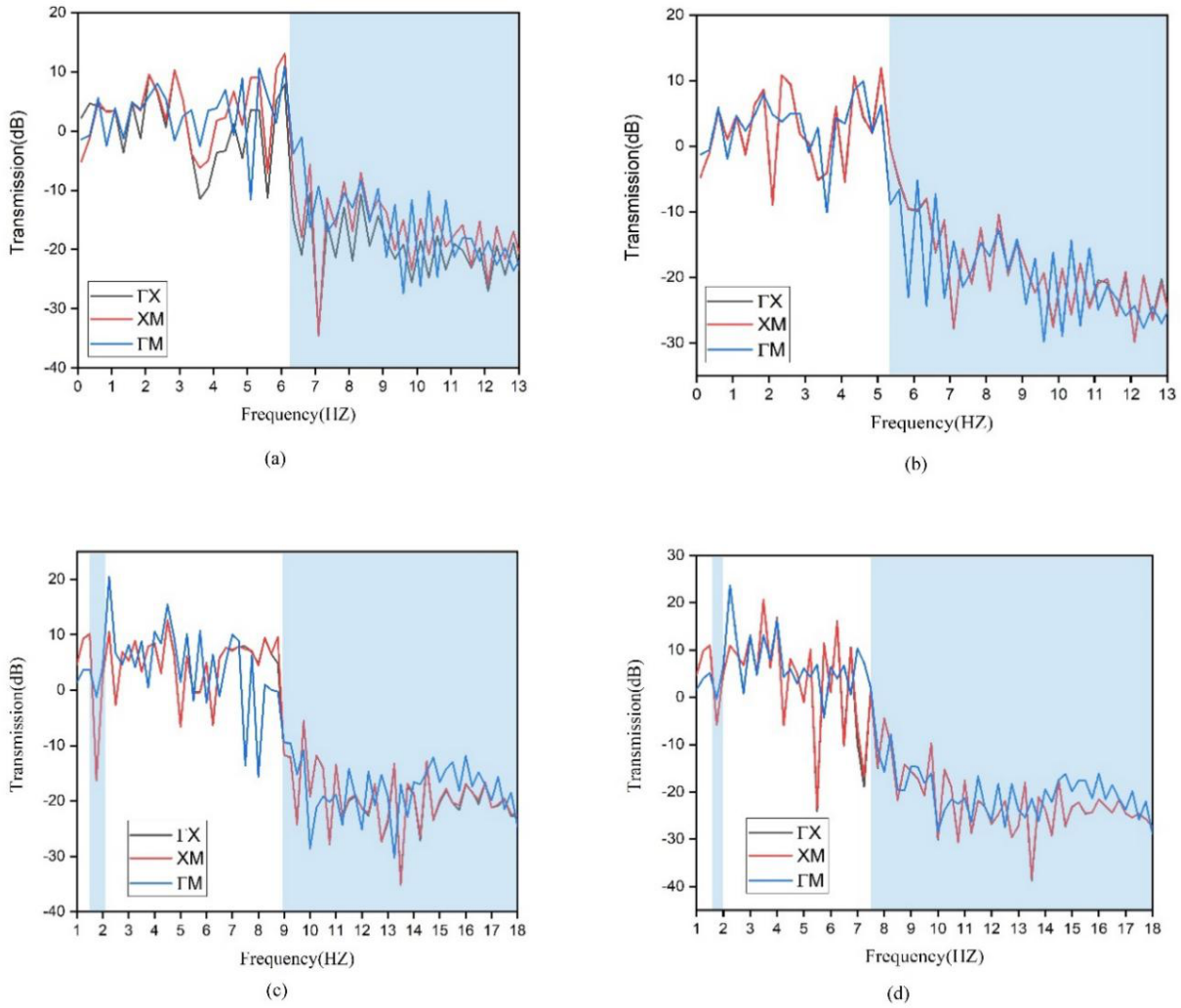

Fig. 9: Transmission spectra for both the samples along with three symmetrical directions of the first IBZ (a)hollow petal-cylindrical SM on the homogenous substrate (b) solid petal-cylindrical SM on the homogenous substrate (c) hollow petal-cylindrical structure on the six-layered substrate(d) solid petal-cylindrical SM on the six-layered substrate.

VI. The influence of geometrical parameters

To further elucidate the influence of resonances in the SM as it plays an imperative part in generating a bandgap, it is relevant to investigate the impact of structural parameters on the bandwidth and position of bandgaps. Here, we take the hollow petal-cylindrical structure on both the homogenous and six-layered soils for example to deliberate the influence of geometric

parameters. Firstly, the effect of the petal's width "*d*" on the bandgap is analyzed. In compliance with the mechanical parameters and geometric parameters keeping constant, when the width *d* of the petals increases from *a/5.5* to *a/3*, the lower boundary of the bandgap slowly moves towards lower frequencies, and the upper boundary almost remains unchanged. Therefore, the relative bandwidth of the BG increases from 0.64 to 0.77 as shown in Fig. 10(a). Secondly, when the outer radius *R* increases from *a/4* to *a/3*, the lower boundary of the BG declines slowly towards lower frequencies, and the upper boundary of the BG almost remains unchanged. Therefore, the relative bandwidth of the BG slightly increases from 0.67 to 0.71 as shown in Fig. 10(b). While, in case of *h*/*a*, as we can see in Fig. 10(c) when the ratio increases from 0.5 to 7.0, the upper edge of the bandgap is almost unchanged or a minor movement towards a lower frequency range can be noticed, and the lower edge moves toward lower frequencies making the bandgap wider. Resultantly, the relative bandwidth of the BG increases from 0.67 to 0.89.

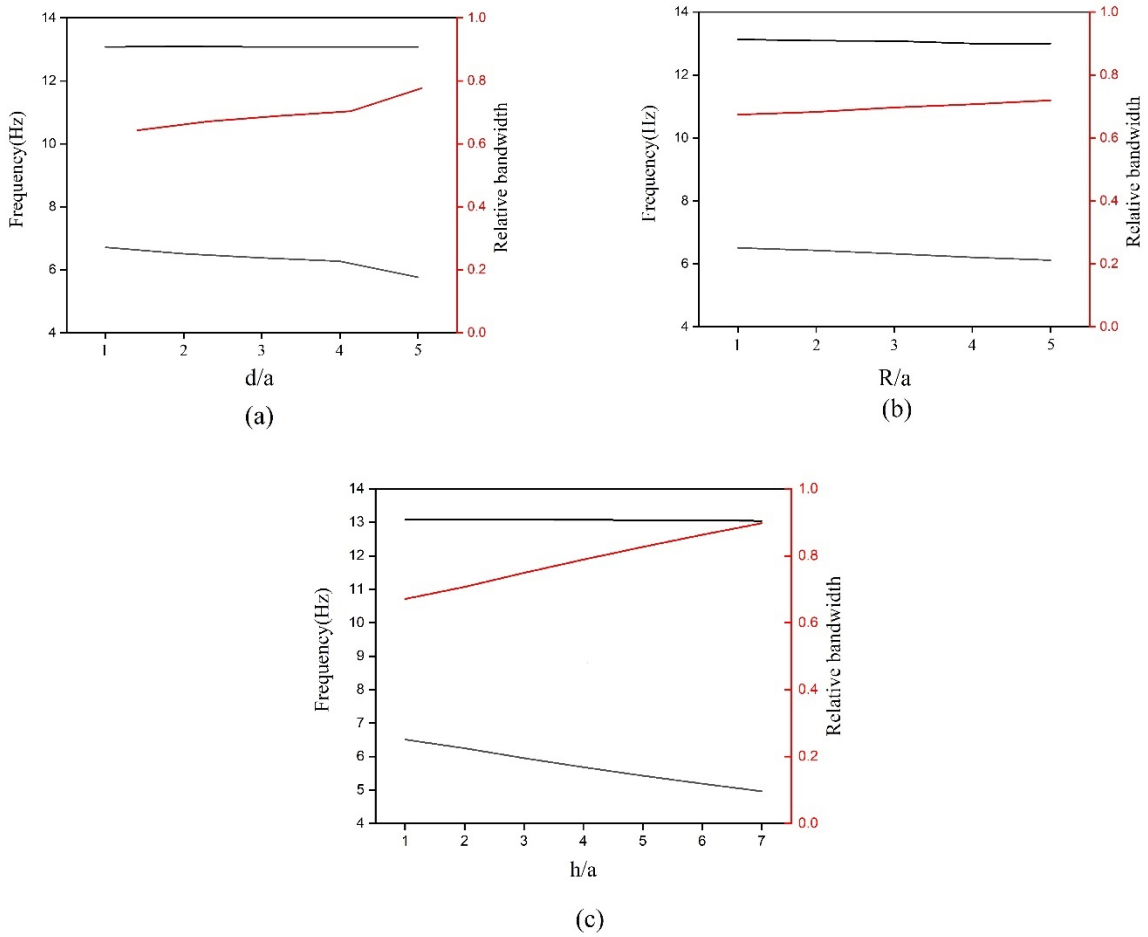

Fig. 10: The geometrical influence for the case of hollow petal-cylindrical SM on a homogenous soil substrate. the ratio of (a) d/a (b) R/a and (c) h/a, the red lines in (a, b and c) are representing the relative bandwidth.

For the second case of hollow petal-cylindrical SM on the stratified soils, a similar effect of geometrical parameters can be noticed as shown in Fig. 11. As the value of *d* increases from *a/4.5* to *a/3*, both the lower and upper edges of the first BG show a negligible movement towards the higher frequency values making a small difference in bandwidth from 1.74 to 1.75. And the lower edge of second BG moves downward and upper edge has a minimal movement towards higher frequencies. And the relative bandwidth changes from 0.72 to 0.78 as we can see in Fig. 11(a). Note that the dotted and solid lines represent the first and second BGs, respectively.

Figure 11(b) shows the influence of variation in the value of *R* on the BGs. As the value of *R* increases from *a/3.75* to *a/3*, both the lower edges of the first BG (dotted lines) and the second BG (solid lines) move slightly towards the lower frequencies, meanwhile, the upper edges move towards lower frequencies. As a result, the relative bandwidth of the first BG (red dotted line) changes from 1.69 to 1.75 and the relative bandwidth of the second BG (solid red line) changes from 0.70 to 0.75 as shown in Fig. 11(b).

Next, as the ratio of *h*/*a* is considered to vary from 0.5 to 7.0, one can notice that the lower and upper edges of the first BG (dotted lines) are slightly moving toward lower frequencies, and the relative bandwidth changes from 1.79 to 1.84. Meanwhile, noticing the second BG (solid lines), we can observe the movement in both the upper and lower edge toward lower frequencies, as a result, the relative bandwidth varies from 0.72 to 0.85.

In short, by changing the geometrical parameters we can tune the bandgap width and position according to a desired range.

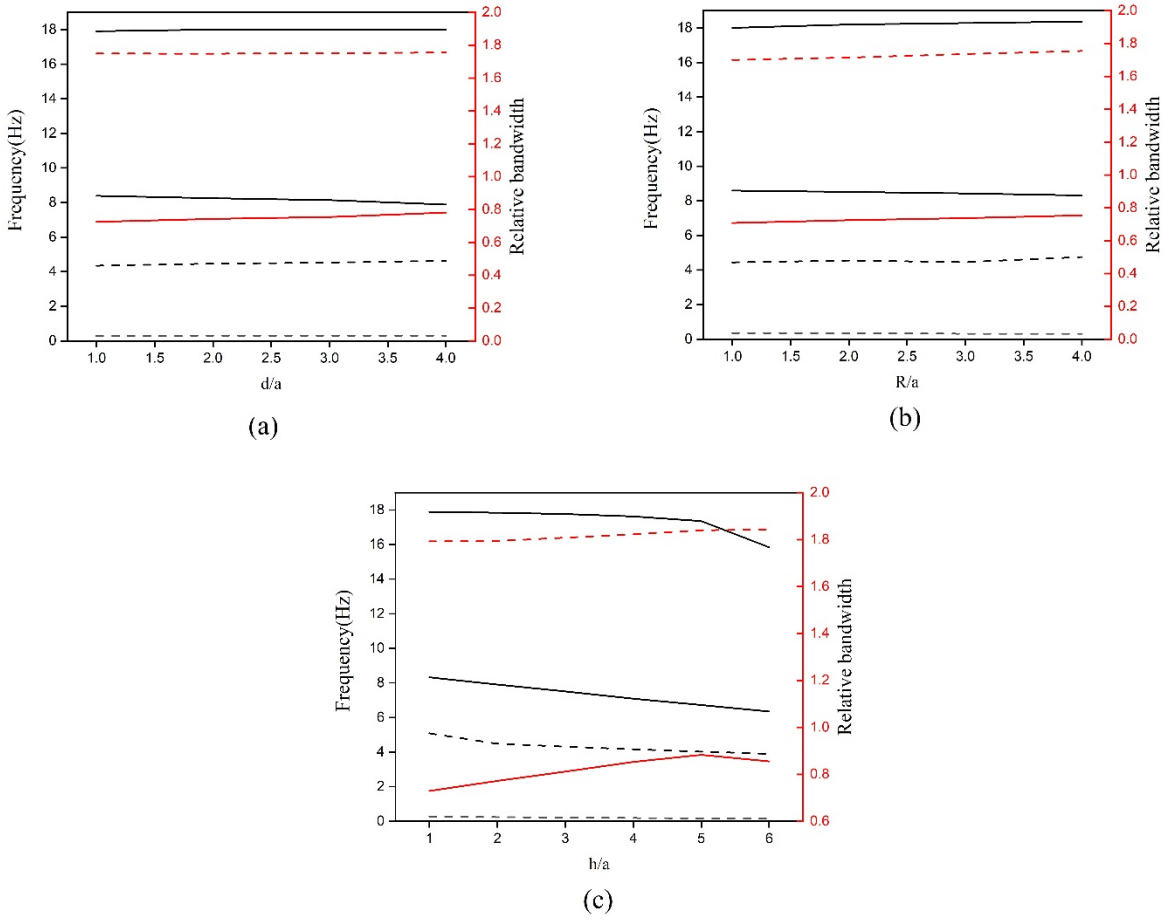

Fig. 11: The geometrical influence for the case of hollow petal-cylindrical SM on a stratified substrate. the ratio of (a) d/a (b) R/a and (c) h/a, the red solid and dotted lines represent the relative bandwidth, black dotted lines indicate first BG and solid black lines indicate second BG.

VII. Material parametric effect

Finally, we considered hollow petal-cylindrical structures evaluating the effect of variation of the mass density and Young's modulus of steel on bandgaps, keeping unchanged for all geometric parameters. As we can see from Figs. 12(a) and (b), for the case of homogenous soil medium Fig. 12(a) while changing the mass density from 1000 (kg/m^3) to 10000 (kg/m^3) one can notice the upper edge remains undisturbed and the lower edge slightly shifts towards the lower frequency range with the increase of mass density of steel. As a result, the relative bandwidth increments from 0.70 to 0.97.

For the case of the layered substrate Fig. 12(b), the lower edge of the second BG (solid

lines) and the upper edge of the first BG (dotted lines) shift towards the lower frequencies, the lower edge of the first BG (dotted lines) and the upper edge of the second BG (solid lines) mostly remain unchanged. Therefore, the relative bandwidth of first BG (dotted lines) shows a very minute difference from 1.755 to 1.757, and the relative bandwidth of second BG (solid lines) increases from 0.72 to 1.00.

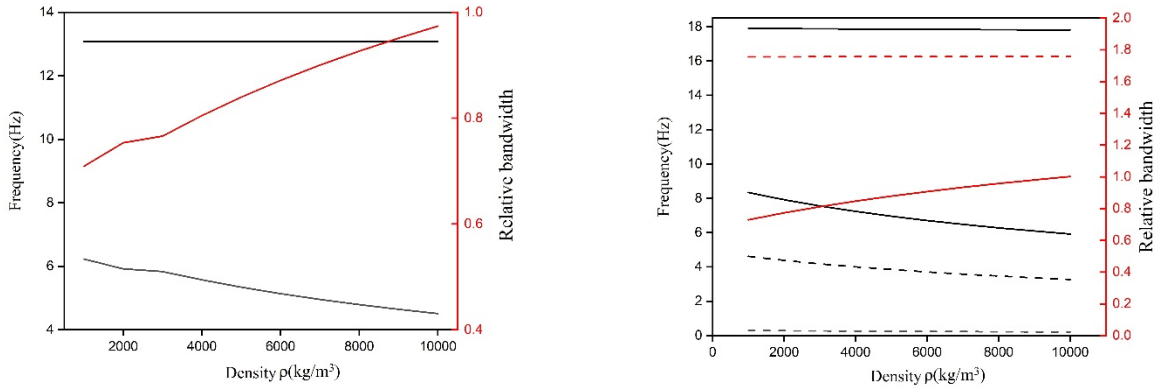

Fig. 12: Effect of material parameters, corresponding to varying mass density ρ(kg/m³) of steel on bandgaps; hollow cylindrical structures on (a)homogenous soil (b) stratified soils.

Moreover, while changing Young's modulus of steel from 50 GPa to 350 GPa, the lower boundary increases slightly and the upper edge remains unchanged for the homogenous soil substrate as shown in Fig. 13(a). Correspondingly, the relative bandwidth decreases from 0.71 to 0.65. For the stratified substrate case, the lower boundary of second BG (solid lines) indicates some movements towards higher frequencies, while the upper edge shows a minute movement toward higher frequencies, and the relative bandwidth (red solid line) decreases from o.75 to 0.66. Whereas, the upper and lower edges of first BG (dotted lines) both remain unchanged, and the relative band width (red dotted line) almost remains undisturbed. In short, the evolution trends of BGs demonstrate that the bandgaps can be set up to the desired position and range by optimizing the material parameters of the structure accordingly and choosing the corresponding material.

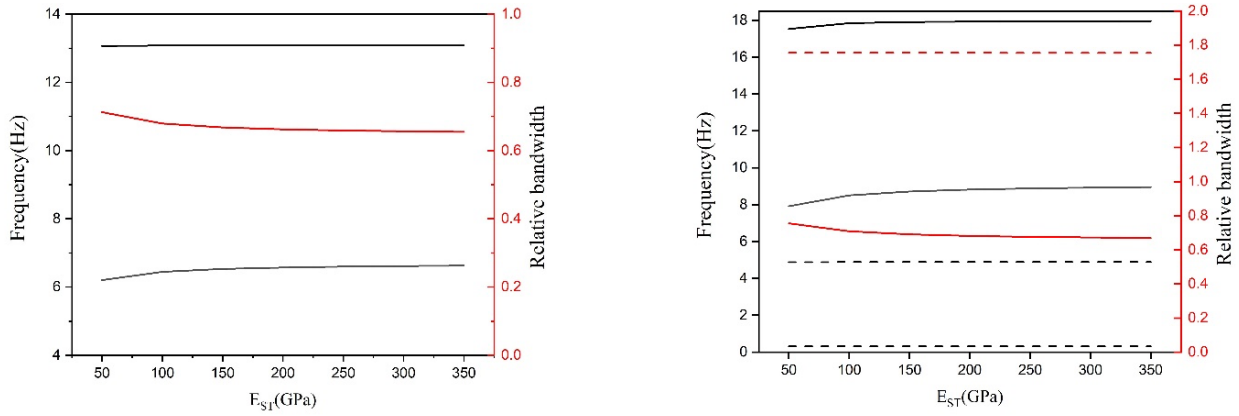

Fig. 13: Influence of Young's modulus of steel on bandgaps for hollow petal-cylindrical SM on (a)the homogenoussoil substrate, (b) six-layered soil substrate.

VIII. Conclusion

This research explores petal-cylindrical SMs, to shield significant civil infrastructures or human structures from earthquake disasters by mitigating low-frequency surface waves. To augment the pragmatism of this research, surface waves propagation through periodically organized petal-cylindrical SM units on both homogenous and six-layered soil substrates are investigated in the finite element method. The generation of bandgaps by local resonance phenomenon from the coupling of the resonator and semi-infinite substrates is calculated and illustrated in band structure graphs. The bandgaps show a great dependence on soil properties. For example, as compared to homogenous soil relatively greater bandwidth can be obtained for stratified soils. through quantifing the transmission in three symmetry directions, the band gaps are further validated by the development of a finite system model. The proposed model for homogenous soil, can provide a bandgap with a relative bandgap width of more than 80% and more importantly, for stratified soils, it can provide not only a bandgap with a relative bandgap width of more than 81% but also a bandgap up to 154%, and can effectively attenuate incident surface waves along three different symmetrical directions. Additionally, the influences of geometrical and material parameters are discussed. Considering practical applications, small geometric sizes and large bandgaps prove that the proposed SMs can be able to offer additional possibilities in the field of seismic hazard prevention.

Acknowledgments

This work was supported by National Natural Science Foundation of China under Grant No: 41974059 and the Key Project of Natural Science Foundation of China under Grant No: 41830537.

Declaration of interest

The authors have no conflicts of interest to declare that are relevant to the content of this article.

Credit Author Statement

Muhammad Muzamil: Conceptualization; Data curation; Formal analysis; Methodology; Software; Roles/Writing - original draft, **Qiujiao Du**: Funding acquisition; Investigation; Project administration; Resources; Supervision; review & editing. **Hongwu Yang:** Visualization; Investigation, **Pai Peng**: Validation; Writing, **Yi Zeng**: Software; Validation, **Rui Xu**: Writing- Reviewing and Editing

Funding source

This work was supported by National Natural Science Foundation of China under Grant No: 41974059 and the Key Project of Natural Science Foundation of China under Grant No: 41830537.

References

[1] S. Brûlé, E.H. Javelaud, S. Enoch, S. Guenneau, Experiments on seismic metamaterials: molding surface waves, Phys. Rev. Lett. 112 (2014) 133901.

[2] A. Sukhovich, L. Jing, J.H. Page, Negative refraction and focusing of ultrasound in two-dimensional phononic crystals, Phys. Rev. B. 77 (2008) 14301.

[3] D.W. Prather, S. Shi, J. Murakowski, G.J. Schneider, A. Sharkawy, C. Chen, B. Miao, R. Martin, Self-collimation in photonic crystal structures: a new paradigm for applications and device development, J. Phys. D. Appl. Phys. 40 (2007) 2635.

[4] A. Khelif, Y. Achaoui, S. Benchabane, V. Laude, B. Aoubiza, Locally resonant surface acoustic wave band gaps in a two-dimensional phononic crystal of pillars on a surface, Phys. Rev. B. 81 (2010) 214303.

[5] P. Sheng, X.X. Zhang, Z. Liu, C.T. Chan, Locally resonant sonic materials, Phys. B Condens. Matter. 338 (2003) 201–205.

[6] G. Wang, X. Wen, J. Wen, L. Shao, Y. Liu, Two-dimensional locally resonant phononic crystals with binary structures, Phys. Rev. Lett. 93 (2004) 154302.

[7] O.R. Bilal, M.I. Hussein, Ultrawide phononic band gap for combined in-plane and out-of-plane waves, Phys. Rev. E. 84 (2011) 65701.

[8] H. Peng, P.F. Pai, H. Deng, Acoustic multi-stopband metamaterial plates design for broadband elastic wave absorption and vibration suppression, Int. J. Mech. Sci. 103 (2015) 104–114.

[9] A. Colombi, R. V Craster, D. Colquitt, Y. Achaoui, S. Guenneau, P. Roux, M. Rupin, Elastic wave control beyond band-gaps: shaping the flow of waves in plates and half-spaces with subwavelength resonant rods, Front. Mech. Eng. 3 (2017) 10.

[10] M. Maldovan, Sound and heat revolutions in phononics, Nature. 503 (2013) 209–217.

[11] J.B. Pendry, Negative refraction makes a perfect lens, Phys. Rev. Lett. 85 (2000) 3966.

[12] R.D. Woods, N.E. Barnett, R. Sagesser, Holography—A new tool for soil dynamics, J. Geotech. Eng. Div. 100 (1974) 1231–1247.

[13] F. Meseguer, M. Holgado, D. Caballero, N. Benaches, J. Sanchez-Dehesa, C. López, J. Llinares, Rayleigh-wave attenuation by a semi-infinite two-dimensional elastic-band-gap crystal, Phys. Rev. B. 59 (1999) 12169.

[14] Z.B. Cheng, Z.F. Shi, Composite periodic foundation and its application for seismic

444 isolation, Earthq. Eng. Struct. Dyn. 47 (2018) 925–944.
445 [15] S. Gonella, A.C. To, W.K. Liu, Interplay between phononic bandgaps and piezoelectric
446 microstructures for energy harvesting, J. Mech. Phys. Solids. 57 (2009) 621–633.
447 [16] F. Fabbrocino, A. Amendola, G. Benzoni, F. Fraternali, Seismic application of pentamode
448 lattices, Ing. Sismica. 33 (2016) 62–70.
449 [17] A. Colombi, P. Roux, S. Guenneau, P. Gueguen, R. V Craster, Forests as a natural seismic
450 metamaterial: Rayleigh wave bandgaps induced by local resonances, Sci. Rep. 6 (2016) 1–
451 7.
452 [18] A. Colombi, D. Colquitt, P. Roux, S. Guenneau, R. V Craster, A seismic metamaterial: The
453 resonant metawedge, Sci. Rep. 6 (2016) 1–6.
454 [19] X. Pu, Z. Shi, Surface-wave attenuation by periodic pile barriers in layered soils, Constr.
455 Build. Mater. 180 (2018) 177–187.
456 [20] Q. Du, Y. Zeng, G. Huang, H. Yang, Elastic metamaterial-based seismic shield for both
457 Lamb and surface waves, AIP Adv. 7 (2017) 75015.
458 [21] M. Miniaci, N. Kherraz, C. Cröenne, M. Mazzotti, M. Morvaridi, A.S. Gliozzi, M. Onorato,
459 F. Bosia, N.M. Pugno, Hierarchical large-scale elastic metamaterials for passive seismic
460 wave mitigation, EPJ Appl. Metamaterials. 8 (2021) 14.
461 [22] A. Mohanty, O.P. Acharya, B. Appasani, S.K. Mohapatra, A broadband polarization
462 insensitive metamaterial absorber using petal-shaped structure, Plasmonics. 15 (2020)
463 2147–2152.
464 [23] L. Chen, Y.-S. Bian, R. Zhou, Large band gaps of petal-shaped acoustic metamaterials based
465 on local resonance, J. Vib. Eng. Technol. 7 (2019) 53–61.
466 [24] G. Gao, N. Li, X. Gu, Field experiment and numerical study on active vibration isolation
467 by horizontal blocks in layered ground under vertical loading, Soil Dyn. Earthq. Eng. 69
468 (2015) 251–261.
469 [25] A. Beiser, Concepts of modern physics, (2021).
470 [26] Y. Zeng, P. Peng, Q.-J. Du, Y.-S. Wang, B. Assouar, Subwavelength seismic metamaterial
471 with an ultra-low frequency bandgap, J. Appl. Phys. 128 (2020) 14901.
472 [27] A. Palermo, S. Krödel, A. Marzani, C. Daraio, Engineered metabarrier as shield from
473 seismic surface waves, Sci. Rep. 6 (2016) 1–10.
474 [28] M. Miniaci, A. Krushynska, F. Bosia, N.M. Pugno, Large scale mechanical metamaterials

as seismic shields, New J. Phys. 18 (2016) 83041.

[29] Y. Xu, R. Xu, P. Peng, H. Yang, Y. Zeng, Q. Du, Broadband H-shaped seismic metamaterial with a rubber coating, EPL (Europhysics Lett. 127 (2019) 17002.